KeAi
CHINESE ROOTS
GLOBAL IMPACT

Available online at www.sciencedirect.com

ScienceDirect

Green Energy & Environment 7 (2022) 742–754

www.keaipublishing.com/gee

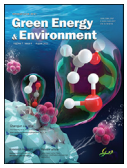

Research paper

The regulating effect of doping Cu on the catalytic performance of CO oxidative coupling to DMO on Pd_xCu_y/GDY: A DFT study

Juan Zhao [a], Min Han [a], Zhanhui Wang [a], Lixia Ling [a,*], Riguang Zhang [b], Baojun Wang [b,*]

[a] College of Chemistry and Chemical Engineering, Taiyuan University of Technology, Taiyuan, 030024, China
[b] Key Laboratory of Coal Science and Technology of Ministry of Education and Shanxi Province, Taiyuan University of Technology, Taiyuan, 030024, China

Received 8 July 2020; revised 14 October 2020; accepted 18 November 2020
Available online 24 November 2020

Abstract

Rely on the density functional theory (DFT) calculation, the catalytic performance of PdxCuy/GDY (x = 1, 2, 3, 4; x + y ≤ 4) for CO oxidative coupling reaction was obtained. The Pd_x/GDY (x = 1, 2, 3, 4) are not ideal catalyst for dimethyl oxalate (DMO) formation because by-product dimethyl carbonate (DMC) is easily formed on Pd_1/GDY and Pd_2/GDY, and high activation energies are needed on Pd_3/GDY and Pd_4/GDY. Therefore the second metal Cu is doped to regulate the performance of Pd_x/GDY (x = 1, 2, 3, 4). Doping Cu not only improve the activity of DMO formation, but more importantly, controlling the ratio of Cu:Pd can effectively regulate the selectivity of DMO. Thus taking into account the activity and selectivity of the reaction for the preparation of DMO by CO oxidative coupling, the Pd_1Cu_1/GDY and Pd_1Cu_2/GDY with the activation energies of 105.2 and 99.2 kJ mol^{-1} to generate DMO show excellent catalytic activity and high DMO selectivity, which are considered as good catalysts for CO oxidative coupling. The differential charge density analysis shows the decrease in the charge density of metal clusters is an important reason for improving the selectivity of the catalyst.

Keywords: GDY; Pd clusters; Cu:Pd ratio; DMO formation; Catalytic performance

1. Introduction

The CO gas phase coupling to generate dimethyl oxalate (DMO) is an efficient and clean reaction, and water is the only by-product during the entire reaction process, which is a green production route [1–4]. Pd-based catalysts exhibit good activity and selectivity for CO oxidative coupling reaction, due to the limited precious metal resources and its high price, considering how to ensure catalytic performance and simultaneously reduce the amount of precious metal Pd becomes the focus of research [5–8]. The Pd nanocrystals with exposed (111) and (100) facets through preferentially oriented facet growth technology were synthesized by Xu et al. [8], and the space-time yield of DMO on Pd (111) surface was much higher than Pd (100) which demonstrated Pd (111) was more favorable for CO oxidative coupling. The CO oxidative coupling to generate DMO on different crystal surfaces of Pd was studied by theoretical calculation, the results showed that the activity sequence of different surfaces of Pd was as follows: Pd (111) (120.6 kJ mol^{-1}) [9] > Pd (100) (129.9 kJ mol^{-1}) > Pd (110) (177.0 kJ mol^{-1}) > Pd (211) (239.6 kJ mol^{-1}) [10]. Therefore, the Pd (111) is selected as judgment standard to screen the catalyst which will applied in DMO generation.

We all know that when the size of the metal particles is reduced to the ultra-small cluster with only a few atoms, the electronic properties of the metal particles will change strongly because of their discrete band structure, so the interactions with the reactants may be different, and the

* Corresponding authors.
E-mail addresses: linglixia@tyut.edu.cn (L. Ling), wangbaojun@tyut.edu.cn (B. Wang).

https://doi.org/10.1016/j.gee.2020.11.011

influence of the number of atoms on the catalytic performance is more significant [11–14]. By adjusting the number of Fe atoms in the catalyst, He et al. precisely controlled the catalytic performance of CO_2 reduction reaction, because the number of Fe atoms can affect its affinity for the key intermediates such as *CO, *CHO, *OCHO and*OCHOH [15]. The study of Pan et al. had shown that the initial conversion rate and product formation rate of glycerol depended on the size of Pt, the average particle size of Pt affected its reaction activity and selectivity [16]. In our previous work [17], the effect of different structures of Pd_n clusters (n = 1, 2, 3, 4, 6) on CO oxidative coupling reaction was studied, and found that Pd_4/TiO_2-O_v showed significantly better catalytic activity than Pd (111), implying the number of atoms greatly influence catalytic performance. Similarly, the DMO generation by CO oxidative coupling was investigated over Pd_n (n = 1, 4, 6) clusters supported on single defect graphene (SVG), and it was found that the active order of Pd_n-SVG (n = 1, 4, 6) catalyst was Pd-SVG ≈ Pd_4-SVG > Pd_6-SVG [18]. Thus, it can be seen that the particle size of the ultrafine cluster with only a few atoms as the catalyst for CO oxidative coupling to DMO affects the catalytic performance.

The interaction of heterogeneous atoms can induce geometric and/or electronic effects to alter the surface adsorption properties and reactivity, changing an atom in a very small cluster is likely to signally alter the electronic structure of the entire cluster and its catalytic properties [19–21]. The propane dehydrogenation reaction was calculated by DFT, and it was found that the monoatomic Pt/CeO_2 catalyst had a strong adsorption capacity to the generated alkenes, so it was not conducive to propylene desorption. But when Sn was added to CeO_2, the PtSn cluster made the product easy to desorption thereby highly improved the selectivity of propylene [22]. Peng et al. [23] studied the influence of Cu^{2+} doping on CO oxidative coupling to DMO, and the small size and high dispersion of Pd nanoparticles promoted by Cu^{2+} ions can explain the phenomenon of the excellent catalytic activity. The influence of core–shell Pd catalyst doped with the second metal Al and Ag on DMO generation was studied by DFT method, indicating that $Al_{13}@Pd_{42}$ can improve the catalytic performance while reducing the amount of Pd [24]. The activity and selectivity of Pd–Cu bimetallic catalyst in selective hydrogenation of acetylene were greatly enhanced by the synergistic action between metals [25]. During the acetone-butanol-ethanol (ABE) condensation, the alloying effect of Cu and Pd leaded to the selectivity of the dehydrogenation reaction which occurred at the PdCu site exceed the decarbonylation reaction [26]. Begum et al. [27] studied the effects of Pd_2 and PdM (M = Cu, Rh, Ag, Au, Pt) dimer catalysts on nitric oxide oxidation, the PdCu bimetallic catalyst showed the lowest activation energy for the rate-determining step because the active Pd-site had stronger ability to activate oxygen.

Because of the poor stability of small metal clusters, they are usually embedded on the surface of metal or carrier to stabilize their existence and prevent agglomeration [28,29]. At the same time, the carrier of the supported metal catalyst can change the reaction performance by affecting the nature of the supported metal [30]. Graphdiyne (GDY) is a planar two-dimensional structure with sp and sp^2 hybridized carbon atoms which formed by the connection of butadiyne and benzene ring, its abundant porous structure can provide space for the deposition of metal clusters, the strong metal–carbon interaction can effectively stabilize metal clusters, and its unique electronic structure is also an important reason to improve the catalytic performance of catalysts [31–33]. It has been reported that GDY can be used as a material for deposition of highly dispersed Pd nanoparticles, and the Pd/GDYO catalyst prepared by chemical deposition has higher catalytic performance than other carbon materials in the reduction reaction of 4-nitrophenol [34]. Similarly, the Pd_1/GDY/G catalyst synthesized by Li et al. had also been proved to have significant catalytic activity and stability for the 4-NP reduction reaction, and the charge transfer of GDY in the catalytic process can effectively improve the activity [35]. Xue et al. [31] had successfully loaded single atom Fe and Ni on GYD, and proved that it can be used as an efficient catalyst for HER reaction. The strong charge transfer between the active site and the carrier was considered to be the reason for the improved catalytic performance. The effects of Mn, Fe, Co and Ni monomers, dimers and trimers fixed on GDY monolayer on N_2 reduction were investigated, the results indicated that all dimers improved catalytic performance compared with Ru (0001) catalyst [36]. The GDY supported $M_xM'_{3-x}$ (M, M' = Ru, Os) bimetallic catalysts had obvious selectivity for the selective hydrogenation of acetylene to ethylene due to the synergy between the bimetals and the interaction between metal clusters and GDY [37]. Research by Shen et al. [38] showed that the catalytic performance of Cu supported on triphenylene-cored graphdiyne for CO_2 electrolytic reduction was better than that of bulk Cu and other Cu-containing catalysts. In addition, metal-modified GDY is not only widely used in the field of catalysis, but also has potential and important application prospects in the fields of electronics and energy, the doping of noble metal atoms (Pd, Pt, Rh and Ir) effectively changes the electronic properties of GDY, making it of great application value in gas molecule sensors [39]. And the Cr- and Mn-doped GDY have spin polarization feature which would be promising used in spintronics devices [40]. The theoretical calculations have proved that light metal (Li, Na, K or Ca) modified GDY or BGDY (boron-graphdiyne) has excellent hydrogen storage performance [41,42].

In this work, we will discuss the reaction mechanism of CO oxidative coupling to produce DMO on Pd_x/GDY (x = 1, 2, 3, 4) to explore the influence of metal clusters of different sizes on the reaction. And in order to obtain an efficient catalyst, doping the second metal Cu to regulate its catalytic performance on DMO generation, this work can provide a reference for the method design of low-cost and high catalytic performance Pd catalysts for CO oxidative coupling to DMO.

2. Computational details

2.1. Calculation methods

In this work, all calculations were carried out by Dmol^3 module in Materials Studio 8.0 [43,44]. The related energy calculation and geometry structural optimization were completed when the energy was converged to 2×10^{-5} Ha (1 Ha = 2625.5 kJ mol^{-1}), the maximum force was converged to 0.004 Ha Å^{-1} (1 Å = 1×10^{-10} m), and the maximum displacement was converged to 0.005 Å. The electronic exchange and correlation functions used generalized gradient approximations (GGA) functional of Perdew, Burke and Ernzerhof (PBE) [45–47]. Symmetry and spin polarization were set to no symmetry and spin unrestricted. Plane-wave electronic density functional theory with long range dispersion interaction corrections DFT-D2 from Grimme [48] was considered to balance computational efficiency and accuracy [49,50]. The *k*-point of the Brillouin zone was set to $3 \times 3 \times 1$ and the global orbital off was set to 4.0 Å. The doubled-numerical quality basis set with polarization functions (DNP) [51,52] was employed with the effective core potentials (ECP) scheme [53,54]. The complete LST/QST method was selected to search the transition states (TS) for every elemental step during the CO oxidative coupling to DMO [55,56]. In the meantime, TS confirmation was carried out to confirm the accuracy of the transition state.

The binding energy between the metal cluster and the support GDY is calculated according to the formula (1):

$$E_b = E_{cluster} + E_{GDY} - E_{cluster/GDY} \quad (1)$$

where the $E_{cluster/GDY}$, $E_{cluster}$ and E_{GDY} represent the energies of GDY after loading the metal cluster, the metal cluster and clean GDY, respectively.

The adsorption energy of related species in the CO oxidative coupling to DMO is calculated by the following formula (2):

$$E_{ads} = E_{catalyst} + E_{adsorbate} - E_{total} \quad (2)$$

where the E_{total}, $E_{catalyst}$ and $E_{adsorbate}$ represent the energies of the system after adsorption, catalyst and the adsorption species in the gas state, respectively.

The activation energy for the elementary reaction is defined as formula (3):

$$E_a = E_{TS} - E_R \quad (3)$$

where E_{TS} and E_R represent the energies of transition state and initial reactant. The heat of reaction (ΔH) is the difference in energy between the products and the reactants in each step of the elementary reaction.

2.2. Models

GDY is a two-dimensional planar network of large conjugated carbon rings containing several alkyne bonds, and has large triangular holes with 18 C atoms (Fig. 1.) [33,57]. To construct the GDY structure, the $2 \times 2 \times 1$ supercell is chosen (a = 18.880 Å, b = 18.880 Å) which contains 72 C atoms, the C–C bond in the benzene ring has a distance of 1.424 Å, the distances of C–C in diacetylenic bond are 1.392, 1.233 and 1.336 Å. The vacuum layer above the GDY surface is 30 Å to avoid interaction between two successive layers along the z axis, the surrounding red C atoms are all fixed during the calculation.

The large triangular hole is selected as the location of metal cluster deposition because previous studies have shown that clusters are more likely to be stable at this location [58]. The Pd_x/GDY (x = 1, 2, 3, 4) are obtained by optimizing the structure of Pd clusters loaded on GDY, and the GDY loaded with metal clusters will undergo minor deformation. Considering the spatial compatibility of metal clusters with GDY structure and the stability of cluster itself [59,60], Pd_4 loaded on GDY is a three-dimensional structure. Furthermore, Pd atoms are replaced with different numbers of Cu atoms to obtain Pd_xCu_y/GDY ($x + y \leq 4$) structures, and the structure optimization was performed for all possible different structures, the most stable structure was selected for subsequent calculations. The most stable PdxCuy/GDY (x = 1, 2, 3, 4; $x + y \leq 4$) structures are shown in Fig. 2.

3. Results and discussion

3.1. Stability of Pd_xCu_y/GDY ($x = 1, 2, 3, 4$; $x + y \leq 4$)

The binding energies of Pd_x (x = 1, 2, 3, 4) and GDY are between 241.4–407.5 kJ mol^{-1}, indicating that Pd_x (x = 1, 2, 3, 4) clusters can stably exist on GDY, which are consistent with previous studies [38,58]. And the binding energies between the Pd_x (x = 1, 2, 3, 4) clusters and GDY increase monotonously with the increase of Pd atoms. The triangular Pd_3 cluster is most similar to the triangular hole of the GDY, while the Pd_4 cluster loaded on GDY is a three-dimensional structure considering the suitability of space, the binding energy of Pd_4 loaded on GDY increases by only 13.2 kJ mol^{-1} and the addition of a fourth atom which will separate Pd_3 from its vantage point near the pore plane [58]. And it can be seen from Table 1 that the binding energies between the bimetal

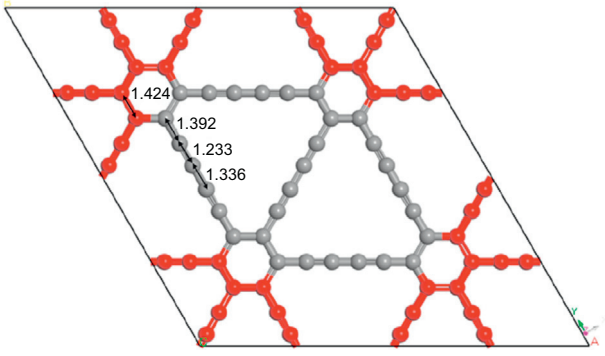

Fig. 1. The GDY structure after optimizing.

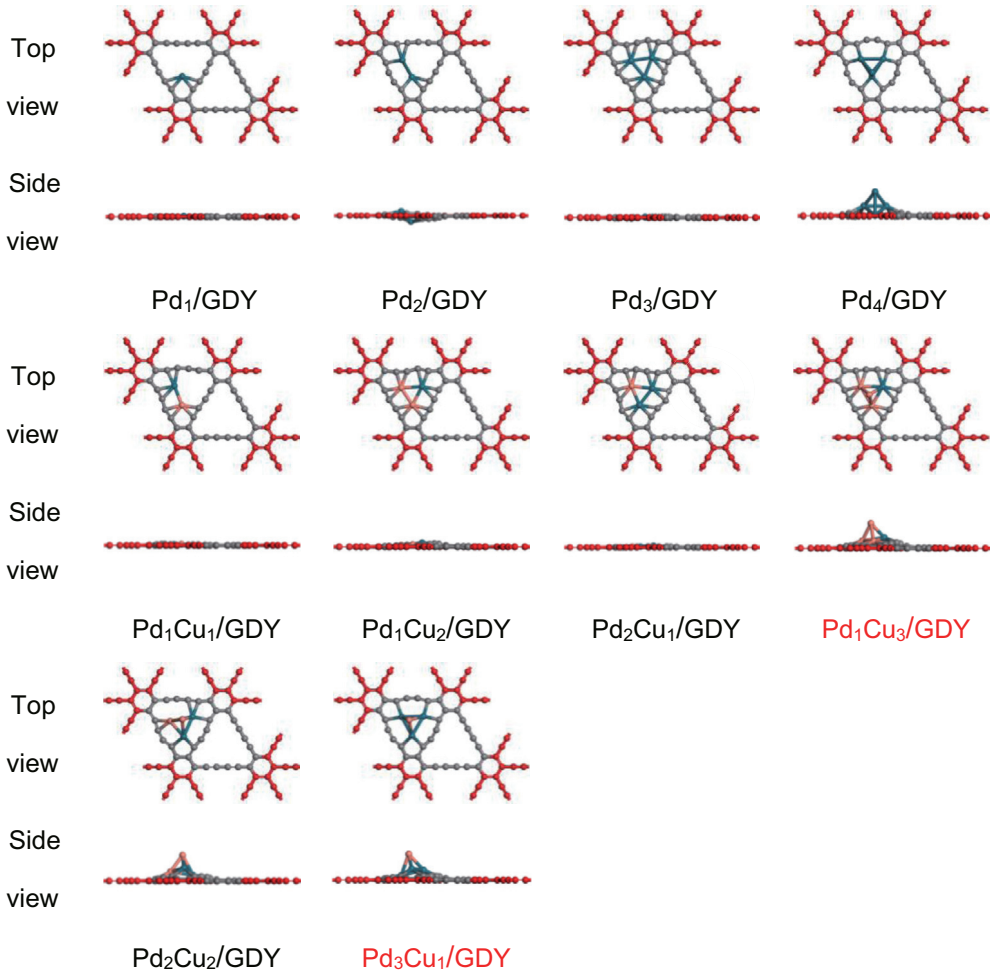

Fig. 2. The most stable configurations of Pd_xCu_y/GDY (x = 1, 2, 3, 4; x + y ≤ 4).

Pd_xCu_y (x + y ≤ 4) clusters and GDY are between 285.8–434.4 kJ mol^{-1}, which is enough to ensure the stable existence of Pd_xCu_y (x + y ≤ 4) clusters on GDY. In addition, the addition of Cu also reduces the sinking distance of the cluster below the GDY monolayer, the bimetal clusters are elevated in the vertical direction compared to before replacement.

3.2. The reaction pathway of CO oxidative coupling to DMO

The DMO is synthesized using CO and methyl nitrite (MN) as the initial reactants by the gas phase method, MN is easily decomposed into NO and OCH_3 because of the small energy of N–O bond [5,61]. Therefore, CO and OCH_3 are used as initial reactants in subsequent studies and the adsorption of species which may participate in the formation of DMO are considered. For CO oxidative coupling to DMO, it can be judged that there are two DMO reaction pathways (Path 1 and Path 2, Scheme 1) by analyzing the adsorption of species on the surface that may participate in the reaction. Since the OCCO intermediate cannot exist stably on Pd_xCu_y/GDY (x = 1, 2, 3, 4; x + y ≤ 4), the way of generating DMO involving OCCO is not considered. Both Path 1 and Path 2 involve the formation of $COOCH_3$, except that C–C bond is

Table 1
The binding energies (E_b) of Pd_x (x = 1, 2, 3, 4) and Pd_xCu_y (x + y ≤ 4) on GDY. The highest distance (h1) of the cluster above the GDY monolayer.

	Pd_1/GDY	Pd_2/GDY	Pd_3/GDY	Pd_4/GDY	Pd_1Cu_1/GDY
E_b (kJ mol^{-1})	241.4	369.1	394.3	407.5	285.8
h1 (Å)	0.063	0.595	0.062	2.685	0.129
	Pd_1Cu_2/GDY	Pd_2Cu_1/GDY	Pd_1Cu_3/GDY	Pd_2Cu_2/GDY	Pd_3Cu_1/GDY
E_b (kJ mol^{-1})	320.5	345.6	434.4	386.3	414.6
h1 (Å)	0.442	0.215	2.908	2.996	3.011

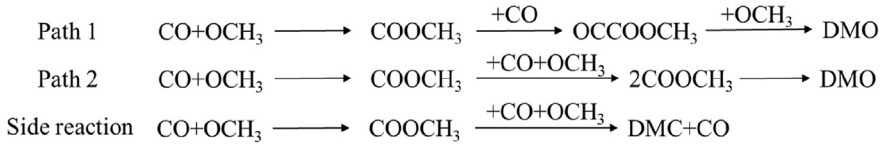

Scheme 1. Pathways of CO oxidative coupling to DMO [9,18,24].

formed in different ways. For the Path 1, $COOCH_3$ reacts with CO to form $OCCOOCH_3$ intermediate. At this time, C–C bond has been formed, and then $OCOCOCH_3$ reacts with OCH_3 to form target product DMO. For the Path 2, two $COOCH_3$ are generated firstly, and then they are coupled as a reactant to generate DMO. In the whole reaction, the formation of by-product dimethyl carbonate (DMC) is also considered to clarify the selectivity of the catalyst for CO oxidative coupling.

3.3. DMO formed by oxidation coupling of CO on Pd_x/GDY (x = 1, 2, 3, 4)

3.3.1. The DMO generation on Pd_x/GDY (x = 1, 2, 3, 4)

For the reaction of CO oxidative coupling to DMO on Pd_1/GDY, because single atom Pd is the active center of the reaction, all species participating in the reaction exist on the catalyst in the way of top adsorption, The potential energy diagram of the reaction and the corresponding structures are shown in Fig. 3. First, the initial reactant CO and OCH_3 are co-adsorbed on Pd_1/GDY, and form a new C–O bond in $COOCH_3$ through the transition state TS1, which needs to cross 88.2 kJ mol^{-1} reaction energy barrier and release heat 56.8 kJ mol^{-1}. After that, the reaction is divided into two paths, the activation energies needed to generate $OCCOOCH_3$ and DMO through Path 1 are 143.0 and 107.1 kJ mol^{-1}, respectively, and the reaction heats are 48.5 and −79.3 kJ mol^{-1}, respectively. The activation energies required to generate the second $COOCH_3$ and the coupling of two $COOCH_3$ to form the DMO in Path 2 are 94.9 and 84.0 kJ mol^{-1}, respectively, and the reaction heats of these two primitive reactions are −107.1 and −14.9 kJ mol^{-1}.

Similar to Pd_1/GDY, the correlation reactions of the two paths of CO oxidative coupling to generate DMO on Pd_2/GDY, Pd_3/GDY and Pd_4/GDY are calculated, the potential energy diagram and the corresponding structures are given at the supporting information, and the activation energy of each primitive reaction is summarized in Table 2. On Pd_2/GDY, CO mainly takes part in the reaction by bridge adsorption, the activation energies required for the first $COOCH_3$ and $OCCOOCH_3$ generation in the reaction are 114.4 and 188.2 kJ mol^{-1}, and the generated $COOCH_3$ and $OCCOOCH_3$ are adsorbed on the top position. The activation energy required for the final elementary reaction of Path 1 to generate DMO is 144.2 kJ mol^{-1}. In Path 2, the energy barrier to be overcome for the second $COOCH_3$ generation is 110.1 kJ mol^{-1}, and the DMO generated by $COOCH_3$–$COOCH_3$ coupling needs to overcome 101.4 kJ mol^{-1}. On Pd_3/GDY, the bridge adsorbed CO and OCH_3 overcame 125.2 kJ mol^{-1} energy barrier to form bridge adsorbed $COOCH_3$. For $CO + COOCH_3 \rightarrow OCCOOCH_3$ and $OCCOOCH_3 + OCH_3 \rightarrow$ DMO in Path 1, the activation energy barriers are 126.6 and 111.4 kJ mol^{-1}, respectively. For $COOCH_3 + CO + OCH_3 \rightarrow 2COOCH_3$ and $OCCOOCH_3 + OCH_3 \rightarrow$ DMO in Path 2, the required activation energies are 168.2 and 144.4 kJ mol^{-1}, respectively. On Pd_4/GDY, the reaction occurs mainly around the Pd atoms at the top of the cluster, after calculating the primitive reaction at each step, it is concluded that it takes 230.4 kJ mol^{-1} to generate DMO through Path 1, and 158.1 kJ mol^{-1} through Path 2.

It can be seen from the above that when x = 1, 2 and 4, the optimal path for DMO generation is $COOCH_3$–$COOCH_3$ coupling path, while the optimal path is CO–$COOCH_3$ path on Pd_3/GDY. Similar to previous studies, when Pd_n is supported on TiO_2-v, the optimal path to generate DMO will change when the number of Pd atoms is different [6]. When x = 1 and 2, the activation energy barriers of the rate-determining steps to generate DMO are 94.9 and 114.4 kJ mol^{-1}, which exhibit higher catalytic activity than the pure Pd (111) (120.6 kJ mol^{-1}) [9]. While the activation energy barriers of rate-determining steps for DMO generation on Pd_3/GDY and Pd_4/GDY are higher than Pd (111) [9].

3.3.2. The DMC generation on Pd_x/GDY (x = 1, 2, 3, 4)

Further, to investigate the selectivity of CO oxidative coupling to generate DMO on Pd_x/GDY (x = 1, 2, 3, 4), the generation of by-product DMC is calculated (Fig. 4.). The formation of DMC starts from co-adsorption $COOCH_3 + CO + OCH_3$, and then formed by the combination of $COOCH_3$ and OCH_3 through the transition state TS6. The energy barriers to be overcome to generate DMC on Pd_x/GDY (x = 1, 2, 3, 4) are 71.2, 102.2, 85.4 and 244.6 kJ mol^{-1}, respectively. Compared with the activation energies of DMO generation (94.9, 114.4, 126.6, 158.1 kJ mol^{-1} on Pd_x/GDY (x = 1, 2, 3, 4)), it can be seen that DMC is easier to be formed on Pd_1/GDY, Pd_2/GDY and Pd_3/GDY. Although Pd_1/GDY and Pd_2/GDY show high catalytic activity, the selectivity is poor and they are not ideal catalyst for DMO synthesis. It is worth mentioning that although the activation energies required to generate DMO is high on Pd_4/GDY, it still shows a good selectivity for the generation of DMO. In summary, it can be seen that the Pd_x/GDY (x = 1, 2, 3, 4) catalyst cannot be both highly active and selective for DMO formation, so they are not recommended for DMO production.

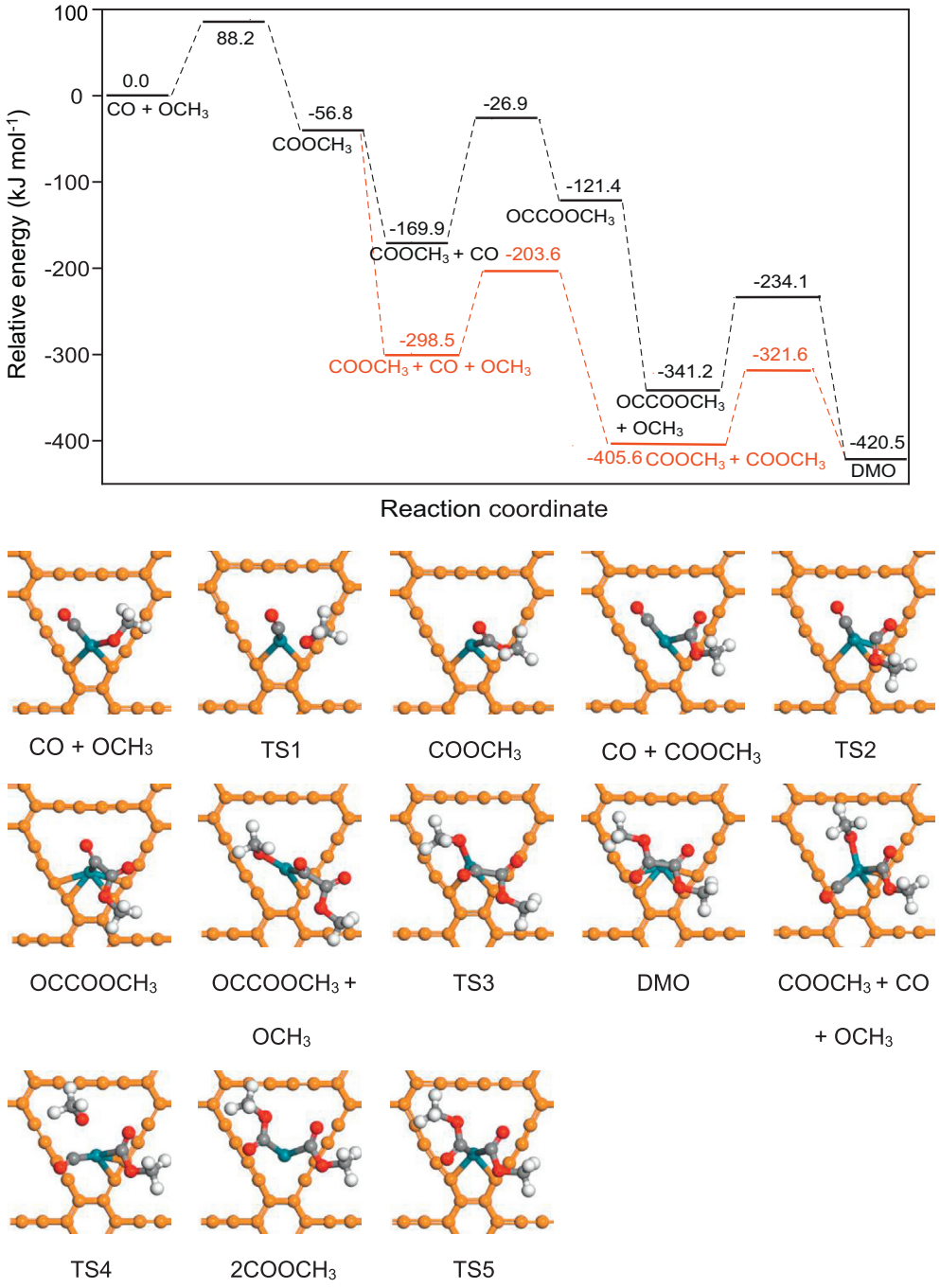

Fig. 3. Potential energy diagram of the reaction of CO oxidative coupling to DMO, as well as structures of initial states, transition states, and final states on Pd_1/GDY. The yellow, dark cyan, gray, red and white represent GDY, Pd, C, O and H, respectively.

Table 2
The activation energy barrier of each primitive reaction for DMO generation on Pd_x/GDY (x = 1, 2, 3, 4). The values are given in kJ mol^{-1}.

primitive reaction		Pd_1/GDY	Pd_2/GDY	Pd_3/GDY	Pd_4/GDY
TS1	$CO + OCH_3 \rightarrow COOCH_3$	88.2	114.4	125.2	158.1
TS2	$CO + COOCH_3 \rightarrow OCCOOCH_3$	143.0	188.2	126.6	230.4
TS3	$OCCOOCH_3 + OCH_3 \rightarrow DMO$	107.1	144.2	111.4	88.7
TS4	$COOCH_3 + CO + OCH_3 \rightarrow 2COOCH_3$	94.9	110.1	168.2	112.2
TS5	$2COOCH_3 \rightarrow DMO$	84.0	101.4	144.4	112.5

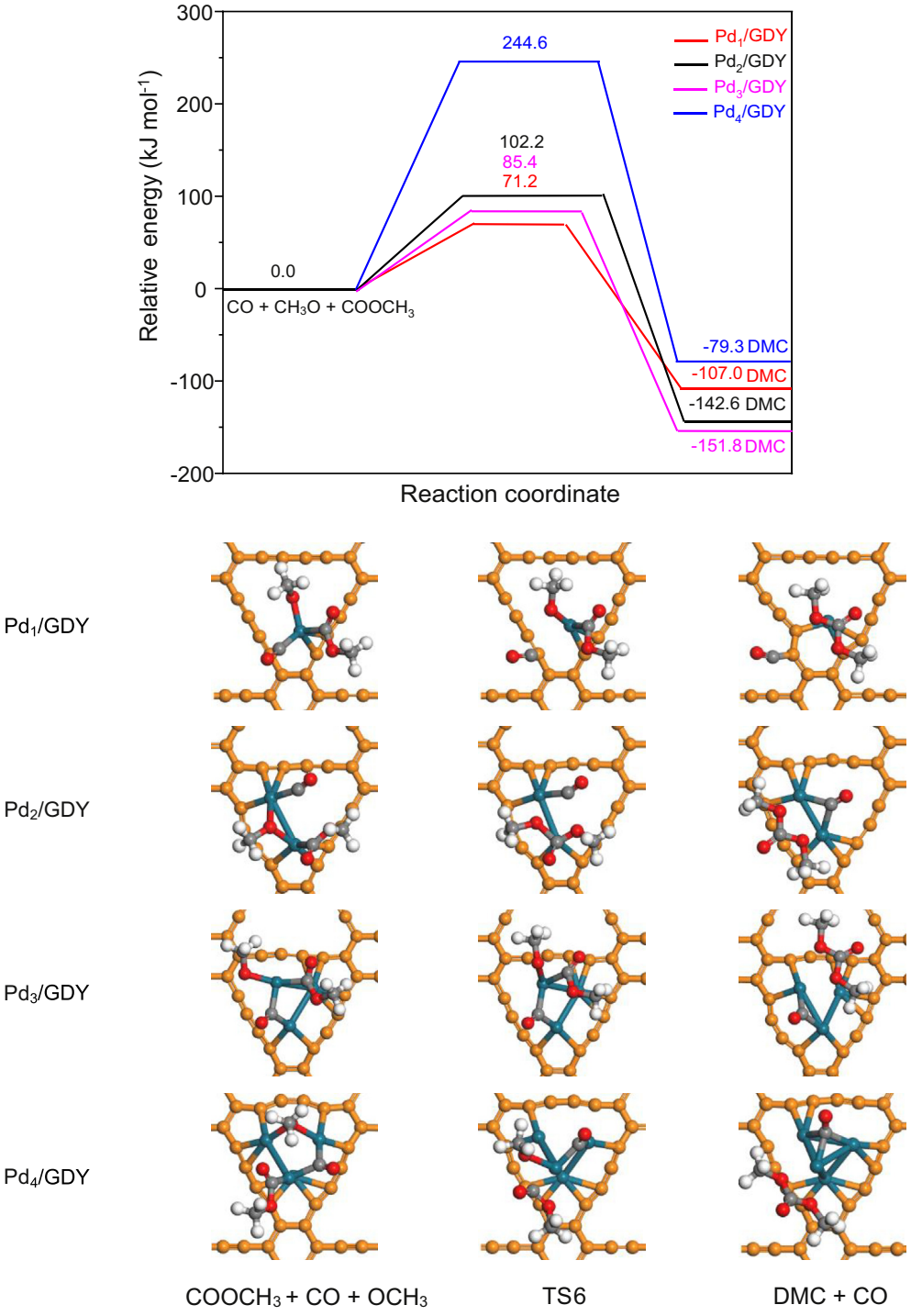

Fig. 4. Potential energy diagram of the DMC generation, as well as structures of initial states, transition states, and final states on Pd_x/GDY (x = 1, 2, 3, 4). The same color scheme is applied as Fig. 3.

3.4. Research on the DMO generation on Pd_xCu_y/GDY ($x + y \leq 4$)

In order to improve the catalytic performance of Pd_x/GDY (x = 1, 2, 3, 4), the second metal Cu is used for modification. For Pd_2/GDY, doping Cu can only form Pd_1Cu_1/GDY with Cu:Pd ratio of 1:1, while for the other two catalysts, due to the different number of substituted Pd atoms, catalysts with Cu:Pd ratio of 1:2, 2:1, 1:3 and 3:1 can be formed, the bimetallic catalyst model is similar to that of Xing et al. [37]. And then CO oxidative coupling reaction on Pd_xCu_y/GDY ($x + y \leq 4$) catalysts with different Pd:Cu ratios are studied, the specific potential energy diagram and the corresponding structures are shown at the supporting information. On Pd_1Cu_1/GDY with

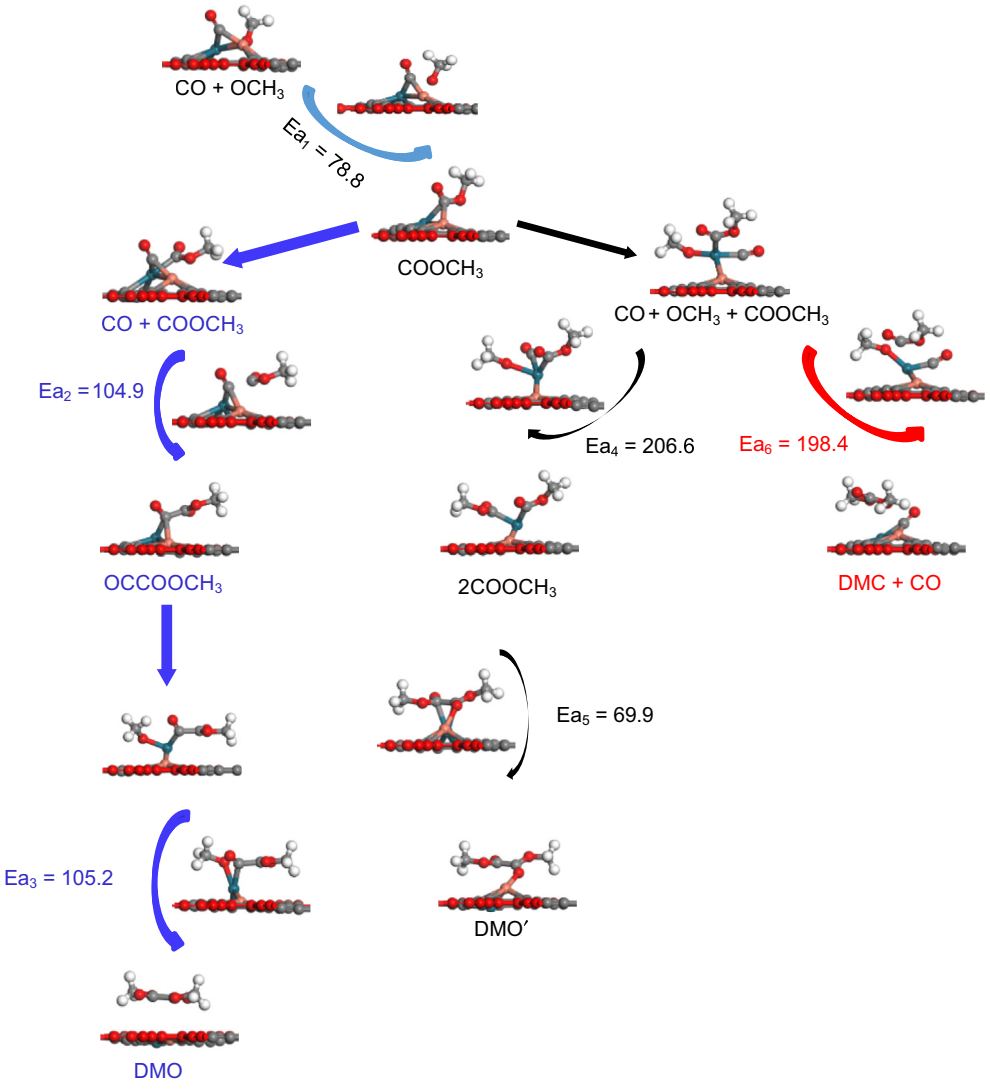

Fig. 5. The activation energy and structure of each element reaction in CO oxidative coupling reaction on Pd_1Cu_1/GDY.

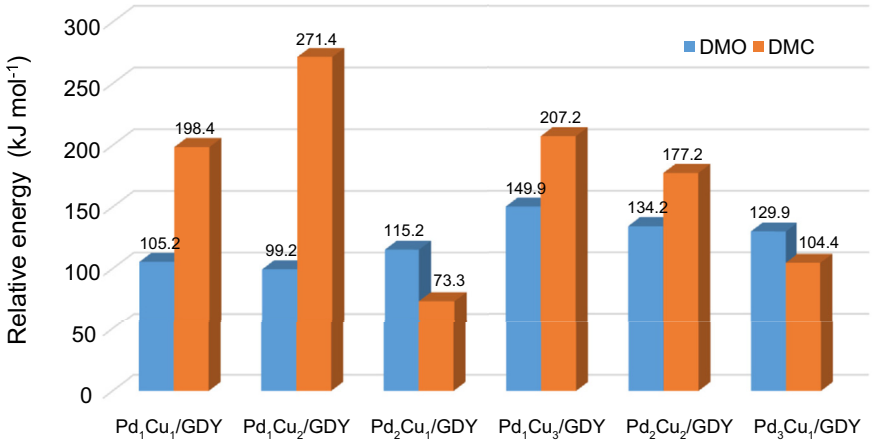

Fig. 6. The activation energy barriers of the rate-determining steps for CO oxidative coupling reaction and the activation energies required for DMC generation on Pd_xCu_y/GDY ($x + y \leq 4$).

the Pd:Cu ratio of 1:1, DMO is more inclined to be generated through the CO–$COOCH_3$ coupling and the rate-determining step is $OCCOOCH_3 + OCH_3 \rightarrow$ DMO whose activation energy is 105.2 kJ mol^{-1} (Fig. 5). Comparing with Pd_2/GDY, it can be seen that the optimal path for CO coupling to DMO after Cu doping is changed, but the activation energy required for generating DMO is reduced, and both are lower than Pd (111). The optimal path of the CO oxidative coupling reaction on Pd_1Cu_2/GDY is Path 2, and Pd_2Cu_1/GDY is the same as those of Pd_3/GDY. The rate-determining steps are $2COOCH_3 \rightarrow$DMO on Pd_1Cu_2/GDY and $OCCOOCH_3 + OCH_3 \rightarrow$ DMO on Pd_2Cu_1/GDY which the activation energies are 99.2 kJ mol^{-1} and 115.2 kJ mol^{-1}, respectively. Similarly compared with Pd_3/GDY, the energy barrier required to generate DMO on Pd_1Cu_2/GDY and Pd_2Cu_1/GDY is sharply reduced. For Pd_1Cu_3/GDY, Pd_2Cu_2/GDY and Pd_3Cu_1/GDY with a three-dimensional metal cluster structure, the activation energies required to generate DMO are 149.9, 134.2 and 129.9 kJ mol^{-1}, the activation energy barrier also goes down relative to Pd_4/GDY (158.1 kJ mol^{-1}). Therefore, it can be concluded that the doping of the second metal Cu with different proportion can increase the activity of Pd_x/GDY (x = 1, 2, 3, 4) to the CO oxidative coupling reaction.

Moreover, in order to better understand the influence of different proportion Cu doping on DMO generation, it is necessary to calculate DMC generation on Pd_xCu_y/GDY ($x + y \leq 4$) (Fig. S9.). By comparing with the activation energies of the rate-determining steps to generate DMO (Fig. 6.), it can be known that DMO is more advantageous on Pd_1Cu_1/GDY, Pd_1Cu_2/GDY, Pd_1Cu_3/GDY and Pd_2Cu_2/GDY. If the activation energies difference between DMO and DMC is used as a descriptor to measure the selectivity of Pd_xCu_y/GDY ($x + y \leq 4$), for catalysts containing the same number of metal atoms, the greater the proportion of Cu atoms, the better the selectivity of the catalyst. As the proportion of Cu in Pd_xCu_y/GDY ($x + y \leq 4$) increases to greater than or equal to 1:1, the DMO becomes more favorable product for CO oxidative coupling reaction.

3.5. General discussion

Based on the above research, the reaction mechanism of Pd_x clusters loaded on GDY for CO oxidative coupling reaction was obtained, and the regulation of the catalytic performance of the second metal Cu doping was explored, the effect of support, particle size and Cu doping were investigated.

3.5.1. The role of GDY as supporter

The larger binding energy between Pd_x (x = 1, 2, 3, 4), Pd_xCu_y ($x + y \leq 4$) and GDY indicates that these metal clusters can exist stably on GDY, it also shows that GDY has an outstanding advantage as an effective carrier of targeted smaller metal catalysts. In order to effectively explore the effect of the GDY on metal clusters, the charge density differences analysis of the catalyst is carried out (Fig. 7.), and the results show that there is an obvious charge exchange among Pd_x (x = 1, 2, 3, 4), Pd_xCu_y ($x + y \leq 4$) metal clusters and GDY. With the increase in the number of atoms of Pd_x (x = 1, 2, 3), there is more charge interaction between Pd_x (x = 1, 2, 3) and GDY, which is also the reason for the increase of the binding energy. When the metal cluster becomes a

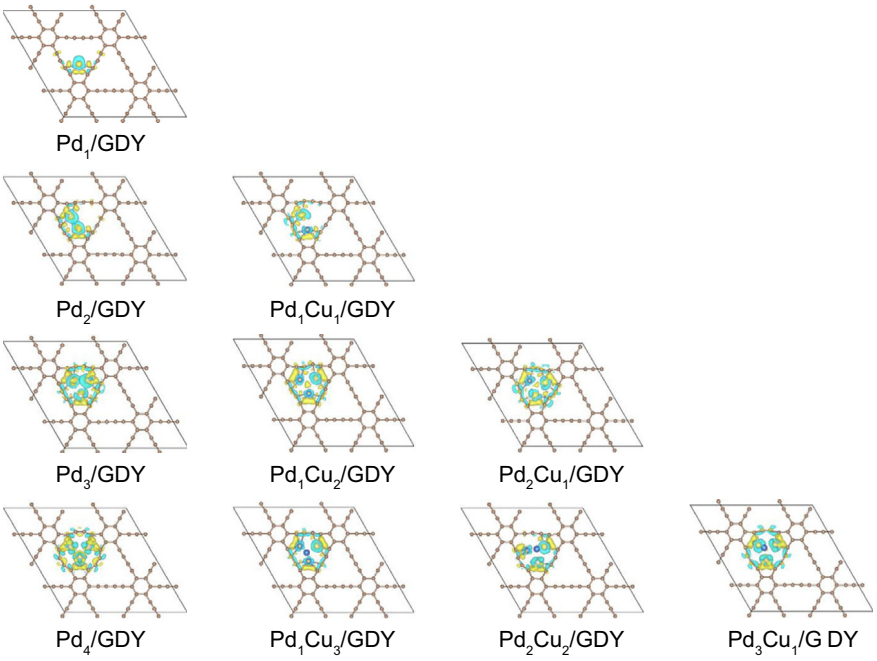

Fig. 7. The charge density differences of Pd_xCu_y/GDY (x = 1, 2, 3, 4; $x + y \leq 4$). Green and yellow represent charge depletion and accumulation, respectively. The values of absolute isosurface is 0.005 e $Å^{-3}$.

tetrahedron, the redistribution of charge is significantly different from Pd_x (x = 1, 2, 3). The addition of the second metal Cu reduces the charge density of the metal clusters and has different catalytic performances for CO oxidative coupling reaction. Concretely, the electron cloud of the metal cluster on Pd_1Cu_1/GDY is significantly smaller than that on Pd_2/GDY, which means that the charge density of the metal cluster on Pd_1Cu_1/GDY is smaller and the charge interaction between GDY is weak, so the binding energy with GDY changes from 369.1 to 285.8 kJ mol^{-1}. A similar phenomenon also occurs on Pd_3, the charge density of the metal clusters decrease with the addition of Cu, and the corresponding binding energy also weakens (394.3, 345.6 and 320.5 kJ mol^{-1} on Pd_3/GDY, Pd_2Cu_1/GDY and Pd_1Cu_2/GDY, respectively). When the number of atoms becomes four, the cluster becomes a three-dimensional structure, and the addition of the fourth atom makes the electronic structure redistribute. Because of the electron redistribution when the number of atoms becomes four, the change of relevant binding energy by Cu substitution is obviously different from that of metal clusters with the number of atoms at two and three. In addition, as the charge density of the metal clusters decreases for the metal clusters with two and three atoms supported by GDY, the process of DMO generation will also change, which will result in different rate determination steps. For instance, the rate-determining step for generating DMO through Path 2 is CO + OCH_3 → $COOCH_3$ on Pd_2/GDY, while on Pd_1Cu_1/GDY is $OCCOOCH_3$ + OCH_3 → DMO through Path 1. Similarly, the favorable path to generate DMO is Path 1 on Pd_3/GDY, but is Path 2 on Pd_1Cu_2/GDY and Pd_2Cu_1/GDY is still Path 1. And the rate-determining step is CO + $COOCH_3$ → $OCCOOCH_3$ on Pd_3/GDY, while are $2COOCH_3$ → DMO on Pd_1Cu_2/GDY and $OCCOOCH_3$ + OCH_3 → DMO on Pd_2Cu_1/GDY. Further, the comparison of the activation energy of the rate-determining step shows that the addition of Cu not only reduce the charge density, but the reaction activity can be improved because the energy barrier of the rate-determining step is significantly reduced. The activation energies of rate-determining change from 114.4 kJ mol^{-1} on Pd_2/GDY to 105.2 kJ mol^{-1} on Pd_1Cu_1/GDY, and go down from 126.6 kJ mol^{-1} on Pd_3/GDY to 115.2 kJ mol^{-1} on Pd_2Cu_1/GDY and 99.2 kJ mol^{-1} on Pd_1Cu_2/GDY. Many studies have also shown that the charge transfer between the GDY and the metal cluster is the reason for the large binding energy and the change of catalytic performance. In previous work, Ag_{38} was stably presented on GDY with a large adsorption energy, and GDY promoted CO oxidative by regulating the electronic structure of metal cluster Ag_{38} which had Ag_4 active site [62].

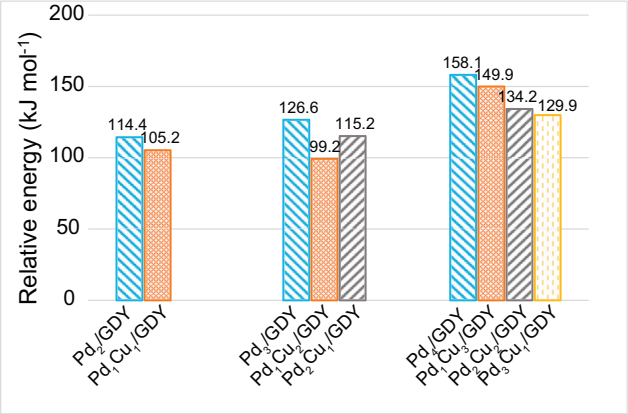

Fig. 8. The activation energy barriers of the rate-determining steps for CO oxidative coupling reaction to DMO on Pd_xCu_y/GDY (x + y ≤ 4).

In addition, Panigrahi et al. [42] discovered that the light metals (Li, Na, K, Ca, Sc, Ti) supported by GDY caused the charge redistribution of the C atoms in GDY, and charge transfer occurred between GDY and metal atoms, which markedly improved the hydrogen storage capacity. And the TM_4/GDY (TM = Sc, Ti, Mn, Fe, Co, Ni and Cu) showed high HER catalytic activity also because the evident electron transfer between the TM_4 and GDY [63].

We further calculate the Hirshfeld charge of the clean GDY and GDY of Pd_xCu_y/GDY (x = 1, 2, 3, 4; x + y ≤ 4) (Table 3), and find that the total charge of clean GDY is 0.0075 e, but after the supported metal clusters, due to the strong interaction between the metal clusters and GDY, a large number of electrons are gathered on the GDY. When Pd_1, Pd_2, Pd_3 and Pd_4 are loaded on GDY, the total charge amount of GDY are −0.3537 e, −0.6131 e, −0.7570 e and −0.7936 e, respectively. The total charge of GDY reduces with the increase of Pd atoms when the number of Pd atoms is 1–4, the more charges on the GDY are accumulated, the smaller the value of total charge, and the greater the binding energy of metal clusters with GDY. In addition, for metal clusters with the same number of atoms, when the cluster contains Cu atoms, the total charge of GDY is higher than that of pure Pd clusters, and it is more obvious when the number of atoms is two and three, which means that Cu will weaken the charge accumulation on GDY.

3.5.2. Effect of cluster size on CO oxidative coupling to DMO

The catalytic activity of CO oxidative coupling to DMO on Pd_x/GDY (x = 1, 2, 3, 4) are analyzed. The activation energy barriers for rate-determining steps of DMO formation are 94.9

Table 3
Hirshfeld charge analysis to obtain the specific charge status of the clean GDY and GDY of PdxCuy/GDY (x = 1, 2, 3, 4; x + y ≤ 4). (e).

	GDY	Pd_1/GDY	Pd_2/GDY	Pd_3/GDY	Pd_4/GDY	Pd_1Cu_1/GDY
Charge	0.0075	−0.3537	−0.6131	−0.7570	−0.7936	−0.5913
	Pd_1Cu_2/GDY	Pd_2Cu_1/GDY	Pd_1Cu_3/GDY	Pd_2Cu_2/GDY	Pd_3Cu_1/GDY	
Charge	−0.6573	−0.7461	−0.7332	−0.7029	−0.7852	

and 114.4 kJ mol^{-1} on Pd_1/GDY and Pd_2/GDY, which perform better catalytic activity compared to Pd (111) [9]. However, Pd_3/GDY and Pd_4/GDY are different from Pd_1/GDY and Pd_2/GDY showing poor activity for the CO oxidative coupling reaction because of their larger activation energy barriers for rate-determining steps, which are 126.6 and 158.1 kJ mol^{-1}. The selectivity of the Pd_x/GDY (x = 1, 2, 3, 4) for CO oxidative coupling reaction is obtained by considering the formation of by-product DMC. Observing the optimal path for DMO generation on these four catalysts, it can find that through $COOCO_3$–$COOCH_3$ coupling path to generate DMO is more favorable on Pd_x/GDY (x = 1, 2, 4), but more likely through CO–$COOCH_3$ coupling path on Pd_3/GDY. When x = 1–3, the final main product is DMC. Although the activation energy barrier to DMO is high on Pd_4/GDY, the DMO is still the main product. From Fig. 7, it can be found that the charge density differences of Pd_4/GDY is obviously different from Pd_x/GDY (x = 1, 2, 3), and the charge density of Pd_4 is significantly lower than that of Pd_x (x = 1, 2, 3), which seems to be the reason for the change in catalyst selectivity.

3.5.3. Effect of doping Cu on the formation of DMO on Pd_x/GDY (x = 1, 2, 3, 4)

The introduction of the second metal Cu aims to regulate the catalytic performance of Pd_x/GDY (x = 1, 2, 3, 4), based on the above research, we find that adding Cu to Pd_2/GDY don't weaken the catalytic activity for CO oxidation coupling reaction, the activation energy barrier of the speed determination step is reduced from 114.4 kJ mol^{-1} on Pd_2/GDY to 105.2 kJ mol^{-1} on Pd_1Cu_1/GDY (Fig. 8). In addition, the addition of Cu significantly reduces the activation energies required for DMO formation on Pd_3/GDY and Pd_4/GDY with poor CO oxidation coupling reaction activity, it goes down from 126.6 kJ mol^{-1} on Pd_3/GDY to 99.2 and 115.2 kJ mol^{-1} on Pd_1Cu_2/GDY and Pd_2Cu_1/GDY which will show better activity compared with Pd (111) [9]. And on Pd_4/GDY, the activation energy required to generate DMO is 158.1 kJ mol^{-1}, also reduces to 149.9, 134.2 and 129.9 kJ mol^{-1} on Pd_1Cu_3/GDY, Pd_2Cu_2/GDY and Pd_3Cu_1/GDY.

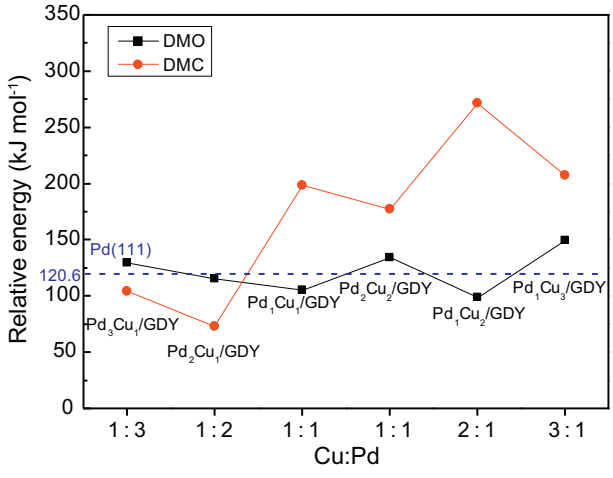

Fig. 9. The activation energies barriers required for the generation of DMO and DMC on Pd_xCu_y/GDY (x + y ≤ 4) with different Cu:Pd ratios.

Similar to the previous calculation process, considering all possible paths to generate DMO, the results show that DMO is generated through the CO–$COOCH_3$ coupling path on Pd_1Cu_1/GDY, Pd_2Cu_1/GDY and Pd_1Cu_3/GDY, and through $COOCH_3$–$COOCH_3$ coupling path on Pd_1Cu_2/GDY, Pd_2Cu_2/GDY and Pd_3Cu_1/GDY. We find that the more the number of doped Cu atoms, the more likely the optimal path for DMO generation will change, the optimal path to generate DMO on Pd_1Cu_1/GDY is different from Pd_2/GDY, on Pd_1Cu_2/GDY is different from Pd_3/GDY, and on Pd_1Cu_3/GDY is different from Pd_4/GDY. Moreover, through the study of the influence of doping second metal Cu on the reaction selectivity, it can be found that the proportion of Pd:Cu on the catalyst is the key factor. There are Pd_1Cu_1/GDY, Pd_2Cu_2/GDY, Pd_1Cu_2/GDY and Pd_1Cu_3/GDY exhibiting excellent selectivity for CO oxidative coupling to DMO (Fig. 9.), as the proportion of Cu in Pd_xCu_y/GDY (x + y ≤ 4) increases to 1:1 or more, the DMO becomes more favorable product for CO oxidative coupling reaction. The introduction of Cu changes the charge distribution of Pd_x/GDY (x = 1, 2, 3, 4) (Fig. 7.), the charge density of the metal clusters is significantly weakened after doping Cu atoms in Pd_x/GDY (x = 2, 3), and the charge is redistributed on Pd_1Cu_3/GDY, Pd_2Cu_2/GDY and Pd_3Cu_1/GDY compared with Pd_4/GDY. The changing of charge density of the metal clusters is also an important internal factor for the change of selectivity, when the charge density of metal clusters is reduced, it is more conducive to improving the selectivity of DMO. Compared with Pd (111) which needs 120.6 kJ mol^{-1} to generate DMO [9], the activation energies required for the formation of DMO on Pd_1Cu_1/GDY and Pd_1Cu_2/GDY with 105.2 and 99.2 kJ mol^{-1} are lower that on Pd (111). Considering the activity of CO oxidative coupling reaction and the selectivity to form DMO, Pd_1Cu_1/GDY and Pd_1Cu_2/GDY can be used for DMO generation.

4. Conclusions

The mechanism of CO oxidative coupling reaction on Pd_xCu_y/GDY (x = 1, 2, 3, 4; x + y ≤ 4) is studied by DFT calculation, the influence of the Pd_x cluster size on the catalytic performance and the regulation of the second metal doping on the catalyst for the DMO generation have been investigated. The results show that the size change of Pd_x cluster will change the optimal path for DMO generation, and the DMO prefers to be formed by $COOCH_3$–$COOCH_3$ coupling path on Pd_1/GDY, Pd_2/GDY and Pd_4/GDY, while by CO–$COOCH_3$ coupling path on Pd_3/GDY. The cluster size also influence the activity and selectivity, among which the catalytic activity is good but more conducive to generate by-product DMC on Pd_1/GDY and Pd_2/GDY, and DMO generation on Pd_3/GDY and Pd_4/GDY is less active than Pd (111), Pd_4/GDY shows better selectivity which may be caused by the decrease of charge density. The Pd_x/GDY (x = 1, 2, 3, 4) cannot guarantee both good activity and selectivity for the formation of DMO, so introduce the second metal Cu to regulate the catalytic performance.

After the introduction of the second metal Cu, the PdCu bimetal clusters can still stably exist on the GDY, but the

charge density of metal clusters are changed. The activation energy barriers of rate-determining steps for CO oxidative coupling reaction are lower compared with before the substitution, which can maintain or even improve the catalytic activity. Moreover, the selectivity of DMO can be adjusted by controlling the Cu:Pd ratio of catalyst, when the ratio of Cu:Pd in the catalyst is smaller than 1:1, it tends to generate the by-product DMC. After comprehensive consideration, Pd_1Cu_1/GDY and Pd_1Cu_2/GDY not only have smaller DMO formation barrier compared with Pd (111), but also have considerable selectivity for DMO formation.

Conflict of interest

We declare that we do not have any commercial or associative interest that represents a conflict of interest in connection with the work submitted.

Acknowledgements

This work is financially supported by the Key projects of National Natural Science Foundation of China (No. 21736007), the National Natural Science Foundation of China (Grant Nos. 21576178 and 21476155), Research Project Supported by Shanxi Scholarship Council of China (No. 2016-030).

Appendix A. Supplementary data

Supplementary data to this article can be found online at https://doi.org/10.1016/j.gee.2020.11.011.

References

[1] S. Uchiumi, K. Ataka, T. Matsuzaki, J. Organomet. Chem. 576 (1999) 279–289.
[2] S.Y. Peng, Z.N. Xu, Q.S. Chen, Z.Q. Wang, D.M. Lv, J. Sun, Y. Chen, G.C. Guo, ACS Catal. 5 (2015) 4410–4417.
[3] C. Wang, Y. Jia, Z. Zhang, G. Zhao, Y. Liu, Y. Lu, Appl. Surf. Sci. 478 (2019) 840–845.
[4] E. Jin, L. He, Y. Zhang, A.R. Richard, M. Fan, RSC Adv. 4 (2014) 48901–48904.
[5] Q. Li, Z. Zhou, R. Chen, B. Sun, L. Qiao, Y. Yao, K. Wu, Phys. Chem. Chem. Phys. 17 (2015) 9126–9134.
[6] L. Ling, Y. Cao, M. Han, P. Liu, R. Zhang, B. Wang, Phys. Chem. Chem. Phys. 8 (2020) 4549–4560.
[7] S.Y. Peng, Z.N. Xu, Q.S. Chen, Z.Q. Wang, Y. Chen, D.M. Lv, G. Lu, G.C. Guo, Catal. Sci. Technol. 4 (2014) 1925.
[8] Z.N. Xu, J. Sun, C.S. Lin, X.M. Jiang, Q.S. Chen, S.Y. Peng, M.S. Wang, G.C. Guo, ACS Catal. 3 (2013) 118–122.
[9] B. Han, X. Feng, L. Ling, M. Fan, P. Liu, R. Zhanga, B. Wang, Phys. Chem. Chem. Phys. 20 (2018) 7317.
[10] L. Ling, H. Lin, B. Han, P. Liu, R. Zhang, B. Wang, Mol. Catal. 470 (2019) 19–31.
[11] J.A. Alonso, Chem. Rev. 100 (2000) 637–678.
[12] M. Boronat, Antonio Leyva-Pérez, A. Corma, Accounts Chem. Res. 47 (2014) 834–844.
[13] L. Liu, A. Corma, Chem. Rev. 118 (2018) 4981–5079.
[14] O. Lopez-Acevedo, K.A. Kacprzak, J. Akola, H. Hakkinen, Nat. Chem. 2 (2010) 329–334.
[15] T. He, L. Zhang, G. Kour, A. Du, J. CO_2 Util 37 (2020) 272–277.
[16] M. Pan, J. Wang, W. Fu, B. Chen, J. Lei, W. Chen, X. Duan, D. Chen, G. Qian, X. Zhou, Green Energy Environ. 5 (2020) 76–82.
[17] Y. Cao, L. Ling, H. Lin, M. Fan, P. Liu, R. Zhang, B. Wang, Comput. Mater. Sci. 159 (2019) 1–11.
[18] L. Ling, X. Feng, Y. Cao, P. Liu, M. Fan, R. Zhang, B. Wang, Mol. Catal. 453 (2018) 100–112.
[19] N. Holmberg, K. Laasonen, P. Peljo, Phys. Chem. Chem. Phys. 18 (2016) 2924–2931.
[20] P. Ferrari, E. Janssens, Appl. Sci. 9 (2019) 16666.
[21] K.J. Taylor, C.L. Pettiette-Hall, O. Cheshnovsky, R.E. Smalley, J. Chem. Phys. 96 (1992) 3319–3329.
[22] H. Xiong, S. Lin, J. Goetze, P. Pletcher, H. Guo, L. Kovarik, K. Artyushkova, B.M. Weckhuysen, A.K. Datye, Angew. Chem. Int. Ed. 56 (2017) 8986–8991.
[23] S.Y. Peng, Z.N. Xu, Q.S. Chen, Y.M. Chen, J. Sun, Z.Q. Wang, M.S. Wang, G.C. Guo, Chem. Commun. 49 (2013) 5718–5720.
[24] X. Feng, L. Ling, Y. Cao, R. Zhang, M. Fan, B. Wang, J. Phys. Chem. C 122 (2018) 1169–1179.
[25] R. Zhang, B. Zhao, L. Ling, A. Wang, C.K. Russelle, B. Wang, M. Fan, ChemCatChem 10 (2018) 2424–2432.
[26] K.A. Goulas, Y. Song, G.R. Johnson, J.P. Chen, A.A. Gokhale, Lars C. Grabow, F.D. Toste, Catal. Sci. Technol. 8 (2018) 314.
[27] P. Begum, R.C. Deka, Catal. Lett. 147 (2017) 581–591.
[28] E. Guan, C.Y. Fang, D. Yang, L. Wang, F.S. Xiao, B.C. Gates, Faraday Discuss 208 (2018) 9–33.
[29] Q. Sun, N. Wang, R. Bai, Y. Hui, T. Zhang, D.A. Do, P. Zhang, L. Song, S. Miao, J. Yu, Adv. Sci. 6 (2019) 1802350.
[30] C. Qiu, Y. Wang, Y. Li, X. Sun, G. Zhang, Z. Yao, S. Deng, J. Wang, Green Energy Environ. 5 (2020) 322–332.
[31] Y. Xue, B. Huang, Y. Yi, Y. Guo, Z. Zuo, Y. Li, Z. Jia, H. Liu, Y. Li, Nat. Commun. 9 (2018) 1460.
[32] D. Malko, C. Neiss, F. Vines, A. Gorling, Phys. Rev. Lett. 108 (2012) 086804.
[33] Y. Li, Y. Li, Acta Phys. Chim. Sin. 34 (2018) 992–1013.
[34] H. Qi, P. Yu, Y. Wang, G. Han, H. Liu, Y. Yi, Y. Li, L. Mao, J. Am. Chem. Soc. 137 (2015) 5260–5263.
[35] J. Li, L. Zhong, L. Tong, Y. Yu, Q. Liu, S. Zhang, C. Yin, L. Qiao, S. Li, R. Si, J. Zhang, Adv. Funct. Mater. 29 (2019) 1905423.
[36] D. Ma, Z. Zeng, L. Liu, X. Huang, Y. Jia, J. Phys. Chem. C 123 (2019) 19066–19076.
[37] D.H. Xing, C.Q. Xu, Y.G. Wang, J. Li, J. Phys. Chem. C 123 (2019) 10494–10500.
[38] H. Shen, Q. Sun, J. Phys. Chem. C 123 (2019) 29776–29782.
[39] Z. Lu, S. Li, P. Lv, C. He, D. Ma, Z. Yang, Appl. Surf. Sci. 360 (2016) 1–7.
[40] X. Chen, P. Gao, L. Guo, Y. Wen, Y. Zhang, S. Zhang, J. Phys. Chem. Solid. 105 (2017) 61–65.
[41] T. Hussaina, B. Mortazavi, H. Bae, T. Rabczuk, H. Lee, A. Karton, Carbon 147 (2019) 199–205.
[42] P. Panigrahi, A.K. Dhinakaran, S.R. Naqvi, R. Gollu, R. Ahuja, T. Hussain, Nanotechnology 29 (2018) 355401.
[43] B. Delley, J. Chem. Phys. 113 (2000) 7756–7764.
[44] B. Delley, J. Chem. Phys. 92 (1990) 508.
[45] I.H. Lee, R.M. Martin, Phys. Rev. B 56 (1997) 7197.
[46] J.P. Perdew, K. Burke, M. Ernzerhof, Phys. Rev. Lett. 77 (1996) 3865–3868.
[47] J.P. Perdew, A. Ruzsinszky, G.I. Csonka, O.A. Vydrov, G.E. Scuseria, L.A. Constantin, X. Zhou, K. Burke, Phys. Rev. Lett. 102 (2009) 039902.
[48] S. Grimme, J. Comput. Chem. 27 (2006) 1787.
[49] W. Jankiewicz, R. Podeszwa, H.A. Witek, J. Chem. Theor. Comput. 14 (2018) 5079–5089.

[50] K. Jiri, M. Angelos, J. Chem. Phys. 137 (2012) 120901.
[51] S. Grimme, J. Comput. Chem. 27 (2006) 1787–1799.
[52] W.J. Hehre, Acc. Chem. Res. 9 (1976) 399–406.
[53] W.J. Hehre, L. Radom, P.R. Schleyer, J.A. Pople, Ab Initio Molecular Orbital Theory, first ed, John Wiley, New York, 1986.
[54] A. Bergner, M. Dolg, W. Küchle, H. Stoll, H. Preu, Mol. Phys. 80 (1993) 1431–1441.
[55] N. Govind, M. Petersen, G. Fitzgerald, D. King-Smith, J. Andzelm, Comput. Mater. Sci. 28 (2003) 250–258.
[56] T.A. Halgren, W.N. Lipscomb, Chem. Phys. Lett. 49 (1997) 225–232.
[57] J. Xi, Y. Nakamura, T. Zhao, D. Wang, Z. Shuai, Acta Phys. Chim. Sin. 34 (2018) 961–976.
[58] A. Seif, M.J. López, A. Granja-DelRío, K. Azizi, J.A. Alonso, Phys. Chem. Chem. Phys. 19 (2017) 19094–19102.
[59] M. Karabacak, S. Özçelik, Z.B. Güvenç, Surf. Sci. 507 (2002) 636–642.
[60] B. Kalita, R.C. Deka, Bull. Catal. Soc. India 5 (2006) 110–120.
[61] C.J. Cassady, B.S. Freiser, J. Am. Chem. Soc. 107 (1985) 1566–1573.
[62] Z.W. Chen, Z. Wen, Q. Jiang, J. Phys. Chem. C 121 (2017) 3463–3468.
[63] R. Ku, G. Yu, J. Gao, X. Huang, W. Chen, Phys. Chem. Chem. Phys. 22 (2020) 3254–3263.